Algorithm for Fast Simultaneous Harmonic and Fundamental Impedance Tuning in Reconfigurable Radar Transmitter Power Amplifiers

Adam Goad
Department of Electrical and Computer Engineering
Baylor University
Waco, USA
Adam_Goad@baylor.edu

Charles Baylis
Department of Electrical and Computer Engineering
Baylor University
Waco, USA
Charles_Baylis@baylor.edu

Paul Flaten
Naval Surface Warfare Center Crane Division
Crane, USA
Paul.Flaten@navy.mil

Brian Olson
Naval Surface Warfare Center Crane Division
Crane, USA
Brian.D.Olson1@navy.mil

Robert J. Marks II
Department of Electrical and Computer Engineering
Baylor University
Waco, USA
Robert_Marks@baylor.edu

***Abstract*—Strategic choice of harmonic load impedances for a radar transmitter power amplifier can increase both the power efficiency and range of the transmitter. With the advent of high-power tunable circuitry, possibilities exist for real-time reconfiguration of the power amplifier fundamental and harmonic impedances to maximize output power and efficiency over changes in frequency and array scan angle. We present, for the first time, a search algorithm that performs simultaneous, fast tuning of the power amplifier fundamental- and harmonic-frequency load impedances. Simulation results demonstrate a 20% PAE increase for the transistor model examined over fundamental tuning alone. In addition, re-tuning after changing frequencies from 500 MHz to 300 MHz is shown to provide a 30% PAE improvement at the second frequency compared to using the same reflection coefficient as the first frequency. These improvements demonstrate the need and benefits of a fundamental and harmonic frequency reconfigurable radar transmitter amplifier in increasing the efficiency and radar range of the transmitter.**

***Keywords*—power amplifier, radar, harmonic tuning, transistor, search algorithm**

I. Introduction

Radar spectrum is becoming increasingly congested, and new techniques continue to emerge for dynamic radar spectrum sharing. Much of the S-band radar allocation in the United States continues to be reallocated, and the 3.45 to 3.7 GHz range is now shared between radar and wireless communications [1]. Cognitive radar systems [2-4] can assess and respond to their environment, and many cognitive radar systems can sense spectrum use and then adjust operating frequency, bandwidth, and the transmitted waveform to coexist with other wireless operations [3, 5-9]. An important part of cognitive radar transmission in spectrum sharing scenarios is the ability to optimize transmission range and efficiency after changing to a new operating frequency. If a tunable matching network is present, such adjustments can be performed in real-time.

It has been shown that power-amplifier output power and power-added efficiency (PAE) can be significantly enhanced by strategic design of load-impedance terminations at harmonic frequencies. Stancliff describes an approach to perform load-pull measurements using harmonic terminations, varying fundamental and harmonic load impedances to maximize the output power or efficiency of a nonlinear power amplifier [10]. Benedikt describes harmonic tuning using a 30 W active load-pull system, where a voltage wave is injected back toward the amplifier to emulate the waveform reflected from a given load impedance. The voltage and current waveforms can be viewed and engineered using an approach called "waveform engineering" to maximize power or efficiency [11]. Vadala describes the use of low-frequency current-voltage measurements to perform characterizations that allow harmonic terminations to be selected [12]. A back-and-forth method of fundamental and harmonic load- and source-pull measurements is demonstrated by Colantonio [13].

Real-time harmonic tuning techniques are useful because narrow-band, tunable matching networks are used rather than wideband, fixed matching networks. Bode [14] and Fano [15] have demonstrated that requiring higher bandwidth theoretically results in degrading the quality of the match [16]. If a network can be designed over a narrow band and adjusted in real-time when the operating frequency is changed to re-optimize performance, then better output power or efficiency at each frequency is likely to be obtained, leading to increased range of the radar and more efficient use of transmitter power supplies.

This work was funded by the Naval Surface Warfare Center – Crane Division under Grant No. N00164-19-1-1002. The views and opinions expressed do not necessarily represent the views and opinions of the U.S. Government.

II. Harmonic Tuning Algorithm

Fast simultaneous tuning of the fundamental and harmonic impedances (related to reflection coefficients) can be performed using the algorithm described in Fig. 1. Fig. 1 shows an illustration of the gradient search in three dimensions for simultaneous fundamental ($\Gamma_{L,1}$) and second-harmonic ($\Gamma_{L,2}$) reflection-coefficient optimization, a concept easily extended to additional dimensions as more harmonics can be tuned. A completely reflective termination is desired for the second-harmonic load impedance because it will prevent power from being delivered to the load at the second-harmonic, reflecting it back into the device and forcing it to be eventually delivered to the load at the fundamental frequency. As such, the optimum second-harmonic reflection coefficient is expected to have a magnitude of 1, and that only phase θ_2 will need to be adjusted, providing a second-harmonic reflection coefficient $\Gamma_{L,2} = 1\angle\theta_2$.

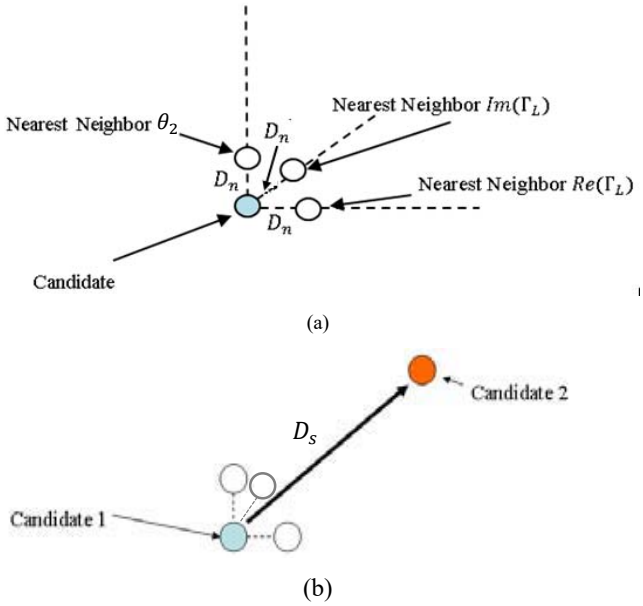

Fig. 1. (a) Visualization of gradient estimation in three-dimensional search space. Neighboring points are used to assess the change in PAE in each dimensional direction, allowing estimation of the gradient. (b) Search step visualization in three-dimensional search. The search proceeds in the direction of the PAE gradient to the next candidate.

At the beginning of the gradient search, neighboring points are measured by varying each by the neighboring-point distance D_n from the initial candidate. The direction of steepest ascent can then be ascertained through a gradient calculation. The search then proceeds in the direction of steepest ascent a predefined search distance, D_s, to the next candidate, as shown in Fig. 1(b). The value of the criterion (*i.e.* PAE) is evaluated at Candidate 2, and if the PAE at Candidate 2 is higher than at Candidate 1, the search process is repeated at Candidate 2. If instead the PAE at Candidate 2 is less than the PAE at Candidate 1, the search distance is divided by two and the shorter search vector is used from Candidate 1 to find a closer candidate in the same direction, and the PAE at this candidate is evaluated. The process carries forward until the search distance is less than the resolution distance, D_r. When this happens, the search is concluded and the point with the highest PAE measured is chosen as the optimum. The progression of the search has been adapted from the steepest-ascent search described by Wilde [16], with some minor changes.

The Smith Tube [17] is a useful tool for visualizing the search progression, and is a three-dimensional extension of the $\Gamma_{L,1}$ Smith Chart. The third (vertical) dimension is used for an additional parameter, as shown in Fig. 2. This search is performed using four parameters: $Re(\Gamma_{L,1})$, $Im(\Gamma_{L,1})$, θ_2, and θ_3. This four-dimensional search can be visualized with two three-dimensional trajectory plots, each plotted in a Smith Tube where the horizontal dimensions are $Re(\Gamma_{L,1})$ and $Im(\Gamma_{L,1})$. For the first Smith Tube, the vertical dimension is θ_2, and for the second Smith Tube, the vertical dimension is θ_3.

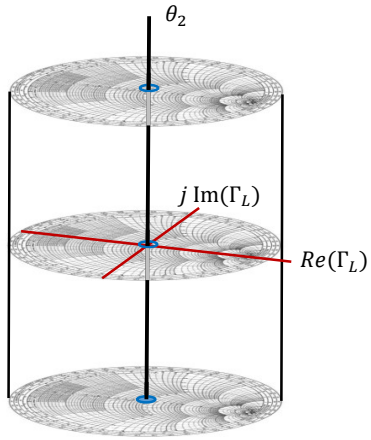

Fig. 2. The Smith Tube [17] is a three-dimensional, cylindrical extension of the Smith Chart, with the third axis representing an additional parameter. Here the third axis represents θ_2, the phase of $\Gamma_{L,2}$.

III. Optimization Search Results

The algorithm was tested experimentally in simulations using Keysight Technologies' Advanced Design System (ADS) microwave circuit simulation software. A Modelithics model for the On Semi MMBFU310LT1 junction field-effect transistor model with V_{GS} = -0.8 V, V_{DS} = 5.75 V was used in a simulation setup allowing independent control of the fundamental, second, and third harmonic impedances.

A. Traditional Harmonic Load-Pull Pre-Design

For comparison with search algorithm results, a traditional harmonic-tuning design approach was used, where fundamental load-pull measurements were first used to select $\Gamma_{L,1}$ to provide the highest PAE with $\Gamma_{L,2} = \Gamma_{L,3} = 1$ (open-circuit harmonic terminations with $\theta_2 = 0°$, $\theta_3 = 0°$). Following this selection, this value of $\Gamma_{L,1}$ was fixed and a second-harmonic load-pull was performed to select $\Gamma_{L,2}$ to further increase PAE to the highest available value. Finally, the selected values of $\Gamma_{L,1}$ and $\Gamma_{L,2}$ were fixed at the determined optimum values and a third-harmonic load-pull simulation was performed to select the value of $\Gamma_{L,3}$ maximizing PAE.

Fig. 3 shows the fundamental load-pull contours that describe the PAE variation over $\Gamma_{L,1}$ with fixed $\Gamma_{L,2} = \Gamma_{L,3} = 1$.

The optimum PAE for fundamental impedance variation is 22.7% at $\Gamma_{L,1} = 0.63/\underline{40.6°}$.

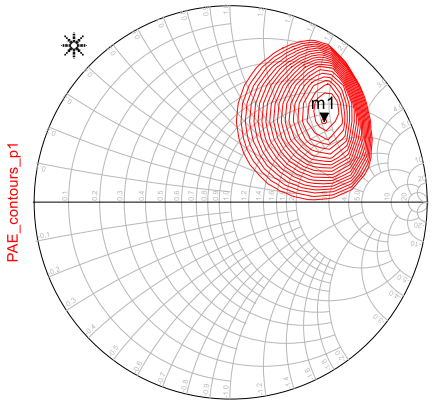

Fig. 3. Traditional 500 MHz simulated fundamental load-pull contours with fixed open-circuit second- and third-harmonic terminations, showing optimum PAE = 22.7% at $\Gamma_{L,1} = 0.63/\underline{40.6°}$, 1.136% PAE step between contours.

Fig. 4 shows the second-harmonic load-pull contours with the fundamental reflection coefficient fixed to the previously determined fundamental optimum ($\Gamma_{L,1} = 0.63/\underline{40.6°}$) and $\Gamma_{L,3} = 1$. The optimum PAE = 40.1% at $\Gamma_{L,2} = 1/\underline{73.0°}$. This termination was then fixed for the second-harmonic, and a third-harmonic load-pull simulation, as shown in Fig. 5, was performed.

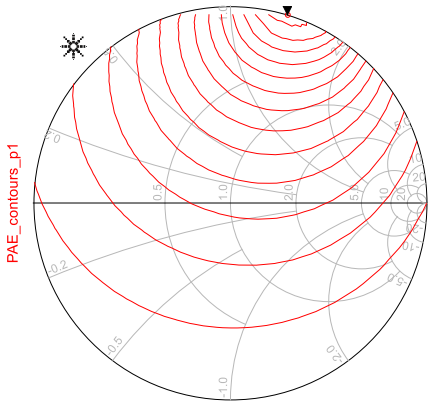

Fig. 4. Traditional 500 MHz simulated second-harmonic load-pull contours with fixed fundamental termination $\Gamma_{L,1} = 0.63/\underline{40.6°}$ and fixed open-circuit third-harmonic termination $\Gamma_{L,3} = 1$, showing optimum PAE = 40.1% at $\Gamma_{L,2} = 1/\underline{73.0°}$, 1.337% PAE step between contours.

The optimum third-harmonic termination was found to be $\Gamma_{L,3} = 1/\underline{79.3°}$. The contours indicate that the best point is slightly inside the Smith Chart but using that point in further calculations provides worse performance than rounding the magnitude to 1. However, the third harmonic termination only increases the PAE by approximately 0.7%, and the second-harmonic termination must have much greater influence than the third harmonic upon device performance for this device and operating conditions. After fixing the second- and third-harmonic terminations to the optima, the fundamental load-pull was re-performed, as shown in Fig. 6, allowing an additional 2% PAE increase. A PAE increase from 22.7% to 45.2% is obtainable by performing harmonic tuning and then re-tuning the fundamental. As such, second-harmonic tuning doubles the efficiency of the transmitter amplifier.

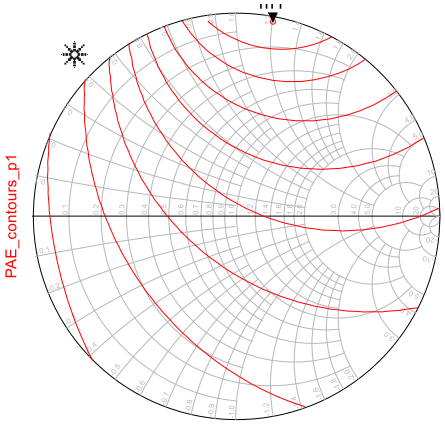

Fig. 5. Traditional 500 MHz simulated third-harmonic load-pull contours with fixed fundamental termination $\Gamma_{L,1} = 0.630/\underline{40.6°}$ and second-harmonic termination $\Gamma_{L,2} = 1/\underline{73.0°}$, showing optimum PAE = 40.8% at $\Gamma_{L,3} = 0.97/\underline{79.3°}$, 0.136% PAE step between contours.

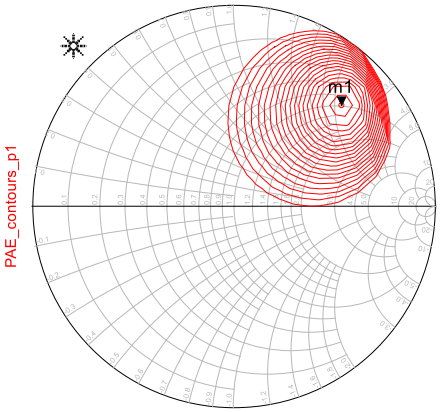

Fig. 6. Traditional 500 MHz simulated fundamental load-pull contours with fixed $\Gamma_{L,2} = 1/\underline{73.0°}$and $\Gamma_{L,3} = 1/\underline{79.3°}$, showing optimum PAE = 45.2% at $\Gamma_{L,1} = 0.73/\underline{43.8°}$, 2.259% PAE step between contours.

B. New Fast Gradient Search for Real-Time Reconfiguration in Frequency-Agile Radar Transmitters

Using the fast gradient search technique of Fig. 1, a search was performed in the four-dimensional space consisting of the four real search parameters $Re(\Gamma_{L,1})$, $Im(\Gamma_{L,1})$, θ_2, and θ_3. A magnitude of 1 was fixed for both the second- and third-harmonic reflection coefficients. Fundamental and harmonic terminations are adjusted simultaneously in the fast search, a feat not accomplishable using the traditional methods.

The search was performed to maximize PAE, and its trajectory is shown in Fig. 7. The search trajectory, as evidenced by Fig. 7(a) and Fig. 7(b), first shows a significant adjustment in the fundamental reflection coefficient (the plane of both Smith Tubes) and then shows a significant upward trajectory in the θ_2 direction, indicating that the second-harmonic phase is adjusted. The third harmonic does not show significant adjustment for this example. For this device, an optimum of 44.5% PAE is obtained at $\Gamma_{L,1} = 0.74/\underline{42.6°}$, $\theta_2 = 73.7°$, and $\theta_3 = -0.66°$ with a total of

66 points assessed (termed "measurements"). Table I compares the fundamental harmonic impedance terminations and performance results of a traditional design versus the fast optimization search. Additionally, the values for $\Gamma_{L,1}$ and θ_2 are very similar to the values found through the traditional sequential design. It appears that θ_3 has little impact on the PAE of the device based on the small additional PAE obtainable from tuning the third harmonic impedance as shown in Fig. 5 (compared to Fig. 4 for second-harmonic termination). As such, it seems the search does not focus much on the optimization of θ_3 since the sensitivity of PAE to θ_3 is low.

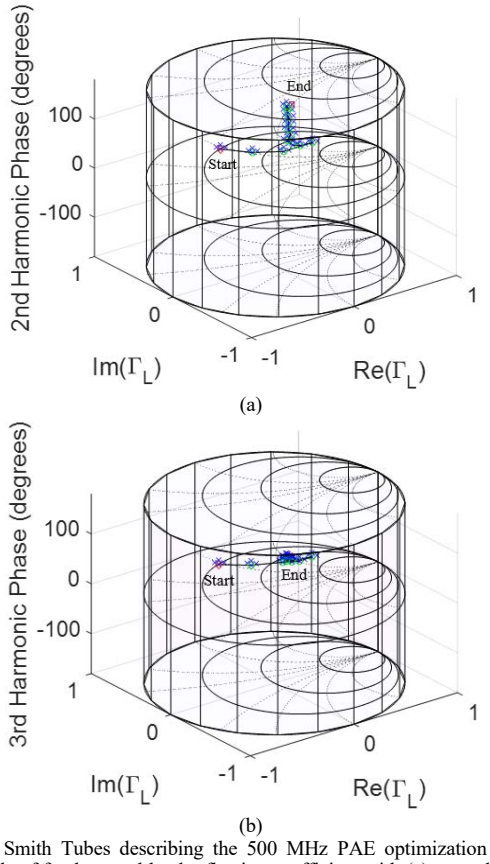

Fig. 7. Smith Tubes describing the 500 MHz PAE optimization trajectory magnitude of fundamental load reflection coefficient with (a) second-harmonic reflection-coefficient phase θ_2 and (b) third harmonic reflection-coefficient phase θ_3. Optimum PAE = 44.5% was obtained at $\Gamma_{L,1}$ = 0.74/42.6°, θ_2 = 73.7°, and θ_3 = -0.66° with a total of 66 measurements.

Fig. 8 shows the progression of PAE and output power during the search of Fig. 7. Fig. 8(a) shows that PAE plateaus at approximately 23%, corresponding with the end of its trajectory parallel to the horizontal plane of the Smith Tube. This part of the search seems to result in a large change in the fundamental termination but negligible change to the second- and third-harmonic phase values. The green triangles in Fig. 8(a) indicate the measured points that represent the highest PAE values measured at or before their measurement numbers. Significant change in the trajectory of the search happens between measurements 25 and 30, and the second-harmonic termination phase begins to be adjusted, providing approximately 45% PAE, an increase of over 20% PAE from the results obtained in the first part of the search, where the primary adjustments were performed on the fundamental termination. In this search, very little adjustment of the third-harmonic reflection coefficient ended up occurring. Notably, the locations of the reflection-coefficient terminations resulting from the fast optimization search are similar to the traditional design results shown in Fig. 6, both in terms of Smith Chart location and maximum PAE achievable, as summarized in Table I. In addition, similar benefits were seen from performing second-harmonic tuning in addition to fundamental tuning.

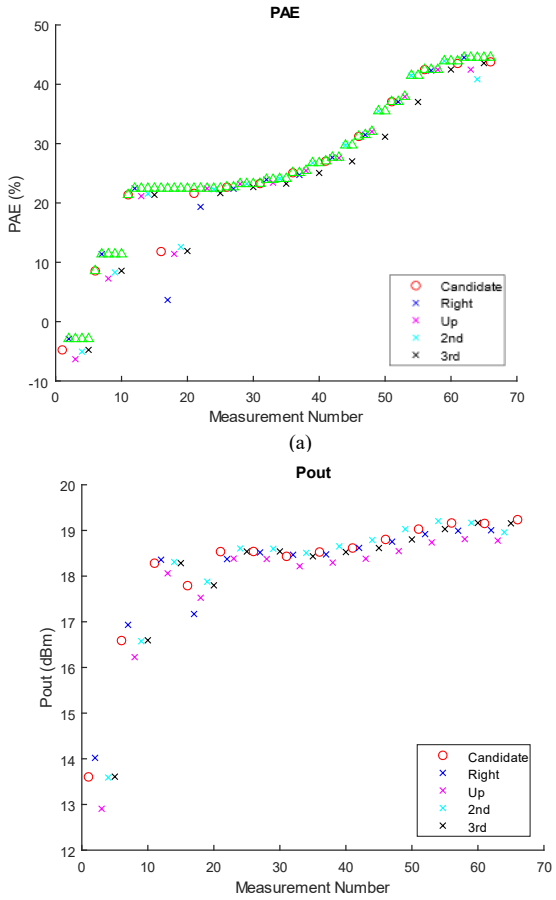

Fig. 8. (a) PAE and (b) amplifier output power P_{out} versus simulated measurement number during the 500 MHz PAE optimization search of Fig. 8

To demonstrate the need for reconfiguration in changing frequencies, a second search was performed at a frequency of 300 MHz beginning at the fundamental and harmonic reflection coefficient values selected as the end point of the first search. Changing frequency while presenting the same reflection coefficients reduces the PAE by 30.0% to 17.3%. The search trajectory is displayed in Fig. 9, starting at the previous frequency's optimum, and shows that the optimum location moves significantly when changing frequency. The algorithm allows reconfiguration to obtain PAE = 47.3% with 31 measurements required for the search. Fig. 10 shows the PAE and output power versus measurement number, and Table I compares the results of this fast search with traditional load-pull design and the fast optimization results at 500 MHz.

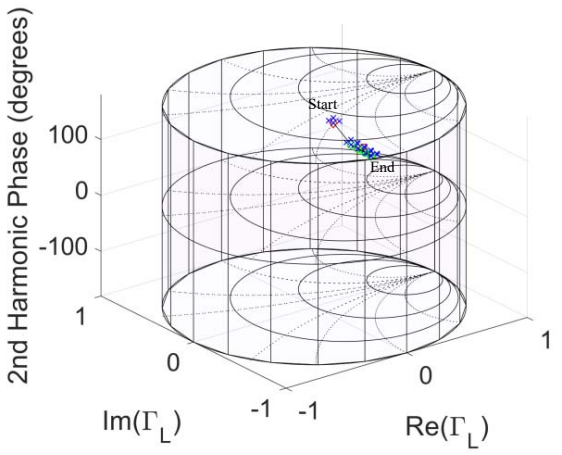

(a)

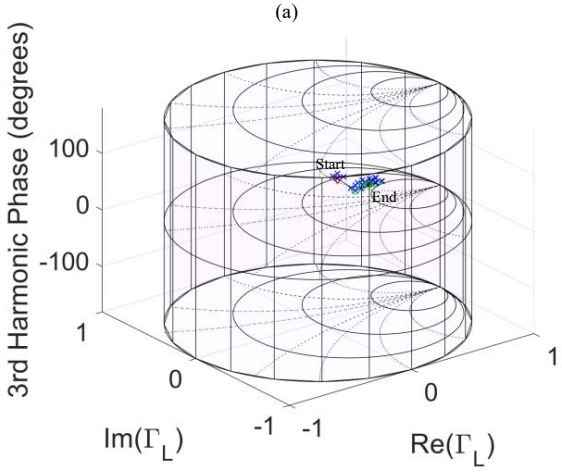

(b)

Fig. 9. Smith Tubes describing the 300 MHz PAE optimization after frequency change trajectory magnitude of fundamental load reflection coefficient with (a) second-harmonic reflection-coefficient phase θ_2 and (b) third harmonic reflection-coefficient phase θ_3. Optimum PAE = 47.3% was obtained at $\Gamma_{L,1}$ = 0.72/25.6°, θ_2 = 36.7°, and θ_3 = -0.95° with a total of 31 measurements.

TABLE I: COMPARISON OF RESULTS FOR TRADITIONAL DESIGN AND FAST PAE SEARCHES AT 500 AND 300 MHZ

	Traditional Design 500 MHz	Fast Search 500 MHz (start from $\Gamma_{L,1}$ = 0.7/90°, θ_2 = 0°, θ_3 = 0°)	Traditional Design 300 MHz	Fast Search 300 MHz (start from 500 MHz optimum $\Gamma_{L,1}$, θ_2, θ_3)
$\Gamma_{L,1}$	0.73/43.8°	0.74/42.6°	0.67/38.5°	0.72/25.6°
θ_2 (°)	73.0°	73.7°	43.1°	38.7°
θ_3 (°)	79.3°	-0.66°	36.3°	-0.95°
Start PAE (%)	-	-12.6%	-	17.3%
End PAE (%)	45.2%	44.5%	49.3%	47.3%
# Meas.	-	66	-	31

An additional search was performed at 500 MHz using the same device and bias settings. For this search, however, output power P_{out} was maximized instead of PAE, which can be directly optimized to maximize radar range. Fig. 11 shows the results of this search, and Fig. 12 shows the PAE and output power during the output-power optimization search.

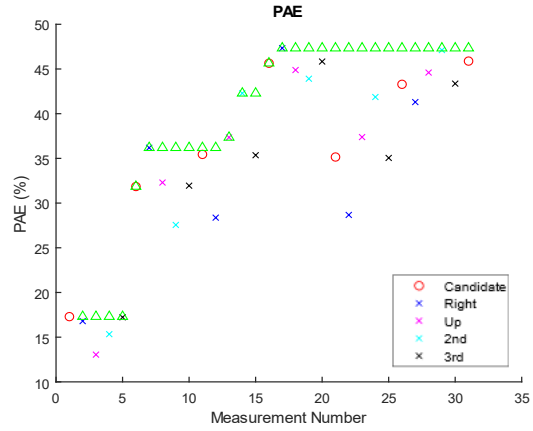

(a)

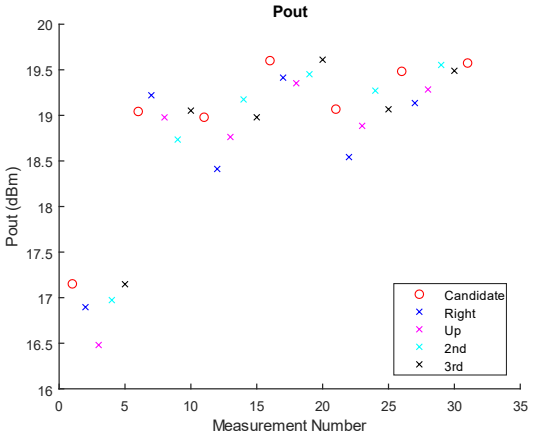

(b)

Fig. 10. (a) PAE and (b) amplifier output power P_{out} versus simulated measurement number during the 300 MHz PAE optimization search after the frequency change shown in Fig. 9.

IV. CONCLUSIONS

A fast real-time search allowing simultaneous optimization of the fundamental and harmonic impedances in a radar transmitter power amplifier has been demonstrated in simulations. Gradient searches to optimize PAE or output power, which is related to radar range, have been demonstrated in the four-dimensional Smith Tube search space. The search results show significant improvement over only optimizing the fundamental reflection coefficient. Next steps include the development of a high-power harmonic tuning network and implementation of the algorithm in tuning this device.

ACKNOWLEDGMENTS

The authors are grateful to Modelithics for the donation of model libraries to Baylor University under the Modelithics University Program.

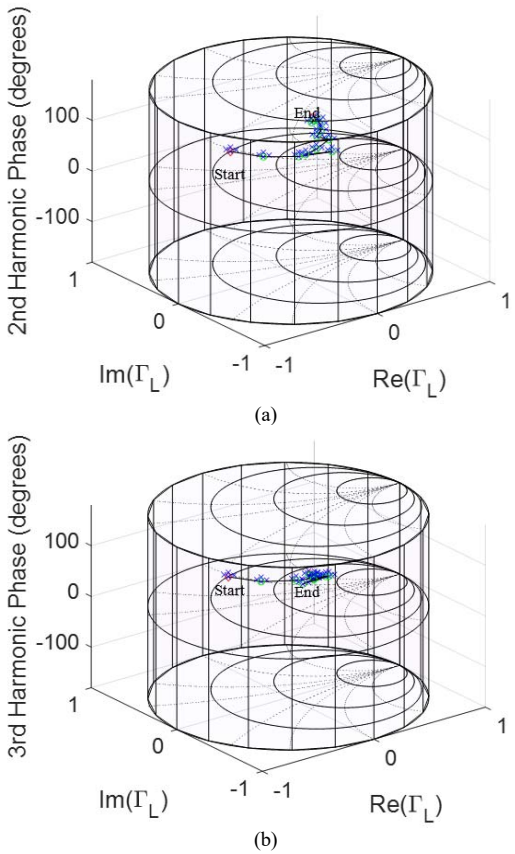

Fig. 11. Smith Tubes describing the 500 MHz output-power optimization trajectory magnitude of fundamental load reflection coefficient with (a) second-harmonic reflection-coefficient phase θ_2 and (b) third harmonic reflection-coefficient phase θ_3. Optimum P_{out} = 19.48 dBm was obtained at $\Gamma_{L,1} = 0.635\angle 38.3°$, $\theta_2 = 62.63°$, and $\theta_3 = 0.09°$ with a total of 61 measurements.

REFERENCES

[1] Federal Communications Commission Rulemaking 12-354: "3.5 GHz Band / Citizens Broadband Radio Service," https://www.fcc.gov/wireless/bureau-divisions/broadband-division/35-ghz-band/35-ghz-band-citizens-broadband-radio.

[2] A.F. Martone, "Cognitive Radar Demystified," *URSI Bulletin*, No. 350, September 2014, pp. 10-22.

[3] S. Haykin, "Cognitive Radar: A Way of the Future," *IEEE Signal Processing Magazine*, January 2006, pp. 30-40.

[4] H. Griffiths, L. Cohen, S. Watts, E. Mokole, C. Baker, M. Wicks, and S. Blunt, "Radar Spectrum Engineering and Management: Technical and Regulatory Issues," *Proceedings of the IEEE*, Vol. 103, No. 1, January 2015, pp. 85-102.

[5] E. Selvi, A. Martone, K. Sherbondy, and R. Buehrer, "On the Use of Markov Decision Processes in Cognitive Radar: An Application to Target Tracking," Proceedings of the 2018 IEEE Radar Conference, Oklahoma City, Oklahoma, April 2018.

[6] G. E. Smith, Z. Cammenga, A. Mitchell, K. L. Bell, J. Johnson, M. Rangaswamy, and C. Baker, "Experiments with Cognitive Radar," *IEEE Aerospace and Electronic Systems Magazine*, Vol. 31, December 2016, pp. 34–46.

[7] B. Kirk, K. Gallagher, J. Owen, R. Narayanan, A. Martone, and K. Sherbondy, "Cognitive Software Defined Radar for Time-Varying RFI Avoidance," Proceedings of the 2018 IEEE Radar Conference, Oklahoma City, Oklahoma, April 2018.

[8] A. Martone, K. Ranney, K. Sherbondy, K. Gallagher, and S. Blunt, "Spectrum Allocation for Non-Cooperative Radar Coexistence," *IEEE Transactions on Aerospace and Electronic Systems*, Vol. 54, No. 1, February 2018, pp. 90 – 105.

[9] A. Aubry, A. De Maio, Y. Huang, M. Piezzo, A. Farina, "A New Radar Waveform Design Algorithm with Improved Feasibility for Spectral Coexistence," *IEEE Transactions on Aerospace and Electronic Systems*, Vol. 51, No. 2, April 2015, pp. 1029-1038.

[10] R.B. Stancliff and D.D. Poulin, "Harmonic Load-Pull," IEEE MTT-S International Microwave Symposium Digest, Orlando, Florida, April/May 1974, pp. 185-187.

[11] J. Benedikt, R. Gaddi, and P.J. Tasker, "High Power Time Domain Measurement System with Active Harmonic Load-Pull for High Efficiency Base Station Amplifier Design," 2000 IEEE MTT-S International Microwave Symposium Digest, Boston, Massachusetts, June 2000, pp. 1459-1462.

[12] V. Vadala, A. Raffo, S. Di Falco, G. Bosi, A. Nalli, and G. Vannini, "A Load-Pull Characterization Technique Accounting for Harmonic Tuning," *IEEE Transactions on Microwave Theory and Techniques,* Vol. 61, No. 7, July 2013, pp. 2695-2704.

[13] P. Colantonio, F. Giannini, e. Limiti, and V. Teppati, "An Approach to Harmonic Load- and Source-Pull Measurements for High-Efficiency PA Design," *IEEE Transactions on Microwave Theory and Techniques*, Vol. 52, No. 1, January 2004, pp. 191-198.

[14] H.W. Bode, *Network Analysis and Feedback Amplifier Design*, Van Nostrand, New York, 1945.

[15] R.M. Fano, "Theoretical Limitations on the Broad-Band Matching of Arbitrary Impedances," *Journal of the Franklin Institute*, Vol 249, pp. 57-83, January 1950, and pp. 139-154, February 1950.

[16] D. Wilde, *Optimum Seeking Methods*, Prentice-Hall, 1964.

[17] M. Fellows, M. Flachsbart, J. Barlow, C. Baylis, and R.J. Marks II, "The Smith Tube: Selection of Radar Chirp Waveform Bandwidth and Power Amplifier Load Impedance Using Multiple Bandwidth Load-Pull Measurements," 2014 IEEE Wireless and Microwave Technology Conference, Tampa, Florida, June 2014.

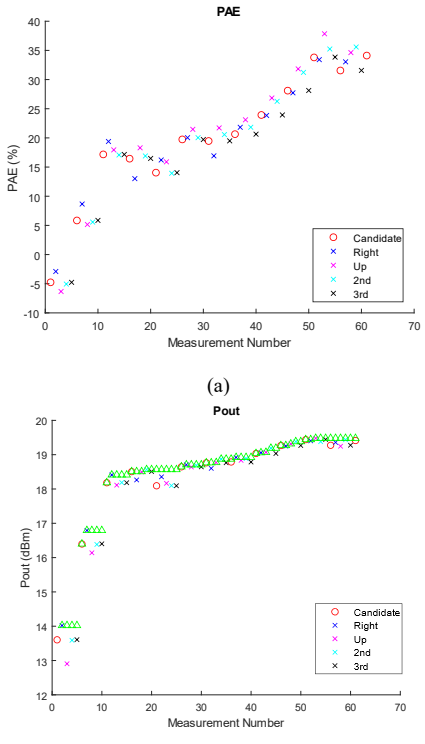

Fig. 12. (a) PAE and (b) amplifier output power P_{out} versus simulated measurement number during the 500 MHz P_{out} optimization search of Fig. 11.